

Conformal invariance in two-dimensional turbulence

D. Bernard[†], G. Boffetta^{*}, A. Celani[•] and G. Falkovich[&]

[†] *Service de Physique Théorique de Saclay,
CEA/CNRS, Orme des Merisiers,
91191 Gif-sur-Yvette Cedex, France*

^{*} *Dipartimento di Fisica Generale and INFN,
Università di Torino,
via Pietro Giuria 1, 10125 Torino, Italy*

[•] *CNRS, INLN, 1361 Route des Lucioles,
06560 Valbonne Sophia Antipolis, France*

[&] *Physics of Complex Systems,
Weizmann Institute of Science,
Rehovot 76100, Israel*

Simplicity of fundamental physical laws manifests itself in fundamental symmetries. While systems with an infinity of strongly interacting degrees of freedom (in particle physics and critical phenomena) are hard to describe, they often demonstrate symmetries, in particular scale invariance. In two dimensions (2d) locality often promotes scale invariance to a wider class of conformal transformations which allow for nonuniform re-scaling. Conformal invariance allows a thorough classification of universality classes of critical phenomena in 2d. Is there conformal invariance in 2d turbulence, a paradigmatic example of strongly-interacting non-equilibrium system? Here, using numerical experiment, we show that some features of 2d inverse turbulent cascade display conformal invariance. We observe that the statistics of vorticity clusters is remarkably close to that of critical percolation, one of the simplest universality classes of critical phenomena. These results represent a new step in the unification of 2d physics within the framework of conformal symmetry.

We consider here 2d incompressible turbulent motion of a fluid, which represents an appropriate description of large-scale motions of the atmosphere and can be realized in different laboratory settings as well¹⁻⁵. As predicted by Kraichnan¹, stirring at some scale L_f results in two turbulence cascades, with the formation of fine-scale vortical structures and large-scale velocity structures. In two dimensions, squared vorticity $\omega^2 = (\nabla \times \mathbf{v})^2$ performs a direct cascade to small scales while kinetic energy $\frac{1}{2}\mathbf{v}^2$ flows from the injection length L_f to large scales, opposite to the three-dimensional case. We focus here on the inverse cascade of energy for which, not surprisingly in view of the presence of a strong interaction, there is no exact analytic theory. Phenomenological dimensional arguments give consistent predictions, though in two seemingly unrelated ways. Consider the velocity difference v_r at the distance r . On the one hand, one may require that the kinetic energy v_r^2 divided by the typical time r/v_r must be constant and equal to the energy flux, ϵ : $v_r^3 \sim \epsilon r$. On the other hand, it can be argued that vorticity, which cascades to small scales, must be in equipartition in the inverse cascade range⁶. If this is the case, the enstrophy $r^d \omega_r^2$ accumulated in a volume of size r is proportional to the typical time r/v_r at such scale, i.e. $r^d \omega_r^2 \sim r/v_r$. Using $\omega_r \sim v_r/r$ we derive $v_r^3 \sim r^{3-d}$ which for $d = 2$ is exactly the requirement of constant energy flux. Amazingly, the requirements of vorticity equipartition (i.e. equilibrium) and energy flux (i.e. turbulence) give the same Kolmogorov-Kraichnan scaling in 2d. Experiments^{4,5,7}

and numerical simulations⁸ indeed demonstrate scale-invariant statistics with the vorticity having scaling dimension $2/3$: $\omega_r \propto r^{-2/3}$.

Our goal here is to find out whether scale invariance can be extended to conformal invariance at least for some properties of 2d turbulence. Under conformal transformations the lengths are re-scaled non-uniformly yet the angles between vectors are left unchanged (a useful property in navigation cartography where it is often more important to aim in the right direction than to know the distance)^{9,10}. The novelty of our approach is that we analyze the inverse cascade by describing the large-scale statistics of the boundaries of vorticity clusters, i.e. large-scale zero-vorticity lines. In equilibrium critical phenomena, cluster boundaries in the continuous limit of vanishingly small lattice size were recently found to belong to a remarkable class of curves that can be mapped into Brownian walk (called Stochastic Loewner Evolution or SLE curves)^{11–19}. Namely, consider a curve $\gamma(t)$ that starts at a point on the boundary of the half-plane H (by conformal invariance any planar domain is equivalent to the upper half plane). One can map the half-plane H minus the curve $\gamma(t)$ back onto H by an analytic function $g_t(z)$ which is unique upon imposing the condition $g_t(z) \sim z + 2t/z + O(1/z^2)$ at infinity. The growing tip of the curve is mapped into a real point $\xi(t)$. Loewner²⁰ found in 1923 that the conformal map $g_t(z)$ and the curve $\gamma(t)$ are fully parametrized by the driving function $\xi(t)$. Almost eighty years later, Schramm¹¹ considered random curves in planar domains and showed that their statistics is conformal invariant if $\xi(t)$ is a Brownian walk, i.e. its increments are identically and independently distributed and $\langle (\xi(t) - \xi(0))^2 \rangle = \kappa t$. In simple words, the locality in time of the Brownian walk translates into the local scale-invariance of SLE curves, i.e. conformal invariance. SLE_κ provide a natural classification (by the value of the diffusivity κ) of boundaries of clusters of 2d critical phenomena¹⁶ described by conformal field theories (CFT)¹⁰ and allow to establish many new results (see [16, 17, 18, 19] for a review).

The fractal dimension of SLE_κ curves is known to be^{22,23} $D_\kappa = 1 + \kappa/8$ for $\kappa < 8$. To establish possible link, let us try to relate the Kolmogorov-Kraichnan phenomenology to the fractal dimension of the boundaries of vorticity clusters. Note that one ought to distinguish between the dimensionality 2 of the full vorticity level set (which is space-filling) and a single zero-vorticity line that encloses a large-scale cluster²⁴. Consider the vorticity cluster of gyration radius L which has the “outer boundary” of perimeter P (that boundary is the part of the zero-vorticity line accessible from outside, see Fig. 3 for an illustration). The vorticity

flux through the cluster, $\int \omega dS \sim \omega_L L^2$, must be equal to the velocity circulation along the boundary, $\Gamma = \oint \mathbf{v} \cdot d\boldsymbol{\ell}$. The Kolmogorov-Kraichnan scaling is $\omega_L \sim \epsilon^{1/3} L^{-2/3}$ (coarse-grained vorticity decreases with scale because contributions with opposite signs partially cancel) so that the flux is $\propto L^{4/3}$. As for circulation, since the boundary turns every time it meets a vortex, such a contour is irregular on scales larger than the pumping scale. Therefore, only the velocity at the pumping scale L_f is expected to contribute to the circulation, such velocity can be estimated as $(\epsilon L_f)^{1/3}$ and it is independent of L . Hence, circulation should be proportional to the perimeter, $\Gamma \propto P$, which gives $P \propto L^{4/3}$, i.e. the fractal dimension of the exterior of the vorticity cluster is expected to be $4/3$.

Let us check this hypothesis by data analysis. A powerful tool for the study of 2d turbulence is the numerical integration of the incompressible Navier-Stokes equations in a planar domain. By this method it is possible to achieve a range of dynamical lengthscales of about four decades, whereas current laboratory experiments are limited to a scale separation of about a hundred. We present here the analysis of very high resolution numerical simulations (with up to 16384^2 grid points) of two-dimensional inverse cascade. (See Table I for the details). Vorticity clusters are shown on Figure 1. The fractal dimension of their exterior boundary (without self-intersections) shown in the left panel of Figure 2 as indeed close to $D_* = 4/3$. Moreover, the fractal dimension of the boundary itself is close to $D = 7/4$. Of course, having some particular dimension does not by itself imply that the curve belong to SLE. Note, however, that the exterior perimeter of SLE_κ with $\kappa > 4$ is conjectured²⁵ to look locally as SLE_{κ_*} curve with $\kappa_* = 16/\kappa < 4$ resulting in the duality relation, $(D-1)(D_*-1) = 1/4$, as observed in our turbulence data. Moreover, $D_* = 4/3$ corresponds to a $\text{SLE}_{8/3}$ curve which represents the continuum limit of a self-avoiding random walk while the dual SLE_6 curve corresponds to a cluster boundary in critical percolation. That prompts us to compare the probability distributions of sizes and boundary lengths between vorticity and percolation clusters. The size s of a cluster is the number of connected sites with the same sign of vorticity, the boundary length b is the number of sites that belong to the cluster but are adjacent to sites of different sign, and the diameter L is the side of the smallest square that covers the cluster. The results shown in the right panel of Fig. 2 are in a good agreement with the exact results from percolation theory.

The two SLEs with $\kappa = 6$ and $\kappa_* = 8/3$ correspond to CFT with zero central charge which means that the scale invariance remains unbroken even when the system is on a

manifold with corners or with a nonzero Euler number (a topological invariant determined by the number of handles and boundaries). Also, SLE_6 curves are singled out by a “locality property” (the curve does not feel the boundary until it touches it), while their dual $\text{SLE}_{8/3}$ has the “restriction property” (the statistics of the curves conditioned not to visit some region is the same as in the domain without this region)^{12–16}. How does all this relate to two-dimensional turbulence?

Now we show by a straightforward check that, within statistical accuracy, large-scale zero-vorticity lines are indeed SLE curves, that is they are conformal invariant and possess remarkable properties of a kind that has never been studied in turbulence. Zero-vorticity isolines that are candidate SLE traces are identified as follows. First, a horizontal line representing the real axis in the complex plane is drawn across the vorticity field. Second, an explorer starting from the origin at the real axis walks on the zero-vorticity isoline keeping the positive vorticity sites always on the right. Third, when the explorer hits the real axis it treads on it always leaving the positive region on its right side until it can re-enter the upper half-plane. This eventually leads the explorer to infinity in an unbounded domain. An example of the outcome of this search is shown in Figure 3. Strictly speaking, this procedure faithfully reproduces all the details of the statistics only if there is a locality property (meaning that the exploration process does not feel the boundary before it hits it), which holds for SLE_6 . Since we obtain as a result SLE with $\kappa \approx 6$, our procedure is self-consistent; we also checked that shifting and turning the line does not modify the results presented below. To determine which driving function $\xi(t)$ can generate such a curve, one needs to find the sequence of conformal maps $g_t(z)$ that map the half-plane H minus the curve into H itself. We approximate $g_t(z)$ by a composition of discrete, conformal slit maps that swallow one segment of the curve at a time (a slight variation of the techniques presented in [26]). This results in a sequence of “times” t_i and driving values ξ_i that approximate the true driving functions. If the zero-vorticity isolines in the half-plane are actually SLE traces, then the driving function should behave as an effective diffusion process at sufficiently large times. We have collected 1,607 putative traces. The data presented by blue triangles in Figure 4 show that the ensemble average $\langle \xi(t)^2 \rangle$ indeed grows linearly in time: the diffusion coefficient κ is very close to the value 6, with an accuracy of 5% (see inset). The average $\langle \xi(t) \rangle$ vanishes by the reflection symmetry of the Navier-Stokes equations. Additionally, the probability distribution functions of $\xi(t)/\sqrt{\kappa t}$ collapse onto a standard Gaussian distribution

at all times t . Therefore, we expect the driving $\xi(t)$ tend to a true Brownian motion and zero-vorticity lines to become SLE_κ traces with κ very close to 6 in the limit of vanishingly small L_f . To appreciate how remarkable this property is, pink symbols in the lower insert in Fig 4 show for comparison the results of the same procedure for the isolines of a Gaussian field having the same Fourier spectrum as vorticity but randomized phases. The slow incomplete recovery to $\kappa = 6$ for the random-phase field occurs at the scales where the power-law correlation is already cut-off by friction and the field becomes truly uncorrelated.

The identification of isovorticity lines as SLE_κ curves allows to apply powerful techniques borrowed from the theory of stochastic differential equations and conformal mapping theory and to obtain analytic predictions for some nontrivial statistical properties of vorticity clusters. The first example is the probability that a point $z = \rho e^{i\theta}$ inside the upper half plane is surrounded by a positive vorticity cluster connected to the positive real axis. In this event, it is not possible to reach infinity with a continuous path starting at z without treading on positive vorticity sites. For this to happen the zero-vorticity line must leave the point z on its right. The probability of such an event depends only on the angle θ between the point and the origin and it assumes a particularly simple form in terms of hypergeometric functions²⁷. In the inset of Figure 5 we show that the analytic solution fits very well the numerical data with $\kappa = 5.9$. The second example is the probability that a vorticity cluster spans the rectangle joining two opposite sides. What is the average number of such spanning clusters? What is the probability that a “four-legged cluster” joins all four sides? By scale invariance these quantities depend only on the aspect ratio r of the rectangle, and their precise dependence can be found by exploiting conformal invariance. In the context of critical percolation formulae for such probabilities have been derived by Cardy²⁸ and Watts²⁹ and later proven by Smirnov³⁰ and Dubédat³¹. In the main frame of Figure 5 we show that numerical data for vorticity clusters follow very closely the expectations for SLE_6 . We have also checked (green symbols in Fig 2) that the dimension of the set of narrow necks that enclose large fjords or large peninsulae has dimension³² $3/4$ (the set is defined by the pairs of points on the curve that are closer than L_f yet separated by an arclength larger than $1000 L_f$). All that gives further support to the result that zero-vorticity lines are conformal invariant and belong to the same class of universality as boundaries of percolation clusters.

Whether the statistics of the zero-vorticity isolines indeed falls into the simplest universality class of critical phenomena (and the fractal dimensions are exactly $7/4$ and $4/3$)

deserves to be a subject of more study. Do our findings signify that universal nature of percolation extends to turbulence as well as to diffusion-limited aggregation³³ and quantum chaos³⁴? At the present level it has the status of a tantalizing conjecture with strong – though not conclusive – support from the data. In view of the non-local constraint imposed by the flow incompressibility, it is quite surprising that the statistics of zero-vorticity isolines (within experimental accuracy) enjoys the locality property inherited by its SLE₆ nature. Remind that continuous percolation can be constructed as a “flooded landscape” determined by some short-correlated random height function. However, vorticity field in the inverse cascade is not short-correlated, it has power-law correlation $\langle \omega(0)\omega(\mathbf{r}) \rangle \propto r^{-4/3}$. When the pair correlation function falls slower than $r^{-3/2}$ then the system is not expected generally to belong to the universality class of uncorrelated percolation and even be conformal invariant³⁵. Indeed, we have seen that the field having the same pair correlation function as the vorticity yet randomized phases of the Fourier harmonics does not have conformal invariant isolines (pink symbols in the lower inset in Fig 4). We thus conclude that there is indeed something special about the vorticity (which has nontrivial phase correlations and higher moments) produced by 2d turbulence. It is also intriguing to notice that conformal field theory of critical percolation possesses a field of scaling dimension $2/3$, identical to the one for the vorticity in Kolmogorov-Kraichnan phenomenology. We may also wonder how conformal invariance is broken in statistical properties of non-zero vorticity isolines. Let us stress that we have found conformal invariance for zero-vorticity isolines, not yet for correlation functions as envisaged by Polyakov³; in the related problem of passive scalar in turbulent flow correlation functions are not conformal invariant^{6,36}.

To conclude, we have developed a numerical tool for testing conformal invariance in physical systems, established this symmetry (within experimental accuracy) for 2d inverse cascade and used it as a powerful new tool in turbulence study which allowed us to make new quantitative predictions confirmed by the experiment. That shows how conformal invariance spans the whole physics, from exalted subjects like string theory and quantum gravity, via statistical mechanics and condensed matter, down to earthly atmospheric turbulence.

-
- [1] Kraichnan, R. H., Inertial ranges in two-dimensional turbulence. *Phys. Fluids* **10**, 1417–23 (1967).
- [2] Kraichnan, R.H. & Montgomery, D., Two-dimensional turbulence. *Rep. Prog. Phys.* **43** 547–619 (1980).
- [3] Polyakov, A. M., The theory of turbulence in two dimensions. *Nucl. Phys.* **B396**, 367–85 (1993).
- [4] Tabeling, P., Two-dimensional turbulence: a physicist approach. *Phys. Rep.* **362**, 1–62, (2002).
- [5] Kellay, H. & I. Goldburg, W., Two-dimensional turbulence: a review of some recent experiments. *Rep. Prog. Phys.* **65**, 845–894 (2002).
- [6] Falkovich, G., Gawedzki K., & Vergassola, M. Particles and fields in fluid turbulence. *Rev. Mod. Phys.* **73**, 913–975 (2001).
- [7] Chen, S. et al On vortex-merger and vortex -thinning in a 2D inverse energy cascade. *57th APS Meeting of the Division of Fluid Dynamics*, abstract MK.009 (Seattle, Washington 2004).
- [8] Boffetta, G., Celani, A. & Vergassola, M., Inverse energy cascade in two-dimensional turbulence: Deviations from Gaussian behavior. *Phys. Rev. E* **61** R29–R32 (2000)
- [9] Polyakov, A. M., Conformal symmetry of critical fluctuations, *JETP Lett.* **12**, 381–3 (1970).
- [10] Belavin, A.A., Polyakov, A.M., & Zamolodchikov, A.A., Conformal field theory. *Nucl. Phys. B* **241**, 333–380 (1984).
- [11] Schramm, O., Scaling limits of loop-erased random walks and uniform spanning trees. *Israel J. Math.* **118**, 221–288 (2000).
- [12] Lawler, G., Schramm, O. & Werner, W., Values of Brownian intersection exponents I: Half-plane exponents, *Acta Math.* **187** 237–273 (2001).
- [13] Lawler, G., Schramm, O. & Werner, W., Values of Brownian intersection exponents II: Plane exponents, *Acta Math.* **187** 275–308 (2001).
- [14] Lawler, G., Schramm, O. & Werner, W., Values of Brownian intersection exponents III: Two-sided exponents, *Ann. Inst. H. Poincare* **38** 109–123 (2002).
- [15] Lawler, G., Schramm, O. & Werner, W., Conformal restriction properties. The chordal case. *Journal Amer. Math. Soc.* **16** 915–955 (2003).
- [16] Lawler, G., Conformally invariant processes in the plane. *Mathematical Surveys and Mono-*

- graphs* **114**, 1–242 (2005)
- [17] Gruzberg I. & Kadanoff, L., The Loewner equation: maps and shapes. *J. Stat. Phys.* **114** 1183–1198 (2004).
- [18] Cardy, J., SLE for theoretical physicists. [arXiv:cond-mat/0503313](https://arxiv.org/abs/cond-mat/0503313).
- [19] Bauer, M. & Bernard, D., Loewner chains. [arXiv:cond-mat/0412372](https://arxiv.org/abs/cond-mat/0412372).
- [20] Löwner, K., Untersuchungen über schlichte konforme Abbildungen des Einheitskreises. *Math. Ann.* **89**, 103–121 (1923).
- [21] Bauer, M. & Bernard, D., Conformal field theories of Stochastic Loewner Evolutions. *Commun. Math. Phys.* **239** 493–521 (2003)
- [22] Saleur, H. & Duplantier, B., Exact determination of the percolation hull exponent in two dimensions, *Phys. Rev. Lett.* **58**, 2325–2328 (1987).
- [23] Beffara, V., The dimension of the SLE curves. [arXiv:math.PR/0211322](https://arxiv.org/abs/math.PR/0211322)
- [24] Kondev, J. & Henley, C., Geometrical exponents of contour loops on Random Gaussian surfaces, *Phys. Rev. Lett.* **74**, 4580–3 (1995).
- [25] Duplantier, B., Conformally invariant fractals and potential theory. *Phys. Rev. Lett.* **84** 1363–1367 (2000).
- [26] Marshall, D. & Rohde, S., Convergence of the Zipper algorithm for conformal mapping. <http://www.math.washington.edu/~marshall/preprints/zipper.pdf>
- [27] Schramm, O., A percolation formula. *Elect. Comm. Probab.* **6**, 115–120 (2001).
- [28] Cardy, J., Critical percolation in finite geometries. *J. Phys. A* **25**, L201–L206 (1992)
- [29] Watts, G., A crossing probability for percolation in two dimensions. *J. Phys. A* **29**, L363–L368 (1996)
- [30] Smirnov, S., Critical percolation in the plane: conformal invariance, Cardy’s formula, scaling limits. *C. R. Acad. Sci. Paris, Sér. I Math.* **333(3)**, 239–244 (2001)
- [31] Dubédat, J., Excursion decompositions for SLE_6 and Watts’ crossing formula. [arXiv:math.PR/0405074](https://arxiv.org/abs/math.PR/0405074).
- [32] Nienhuis, B., Exact critical point and critical exponents of $O(n)$ models in two dimensions. *Phys. Rev. Lett.* **49** 1062–1065 (1982).
- [33] Meakin, P. & Family, F., Diverging length scales in diffusion-limited aggregation. *Phys. Rev. A* **34** 2558–2560 (1986).
- [34] Bogomolny, E. & Schmit, C., Percolation Model for Nodal Domains of Chaotic Wave Func-

tions. *Phys. Rev. Lett.* **88** 114102 (2002).

[35] Weinrib A., Long-correlated percolation, *Phys. Rev. B* **29**, 387–95 (1984).

[36] Falkovich, G. & Fouxon, A., Anomalous scaling of a passive scalar in turbulence and equilibrium. *Phys. Rev. Lett.* **94**, 214502 (2005).

Acknowledgements This work was supported by the grants from the European network and Israel Science foundation. G.F. thanks A. Zamolodchikov, A. Polyakov, E. Bogomolny and K. Gawedzki for useful discussions.

Author Information Reprints and permissions information is available at npg.nature.com/reprintsandpermissions. The authors declare that they have no competing financial interests. Correspondence and requests for materials should be addressed to G.F. (gregory.falkovich@weizmann.ac.il).

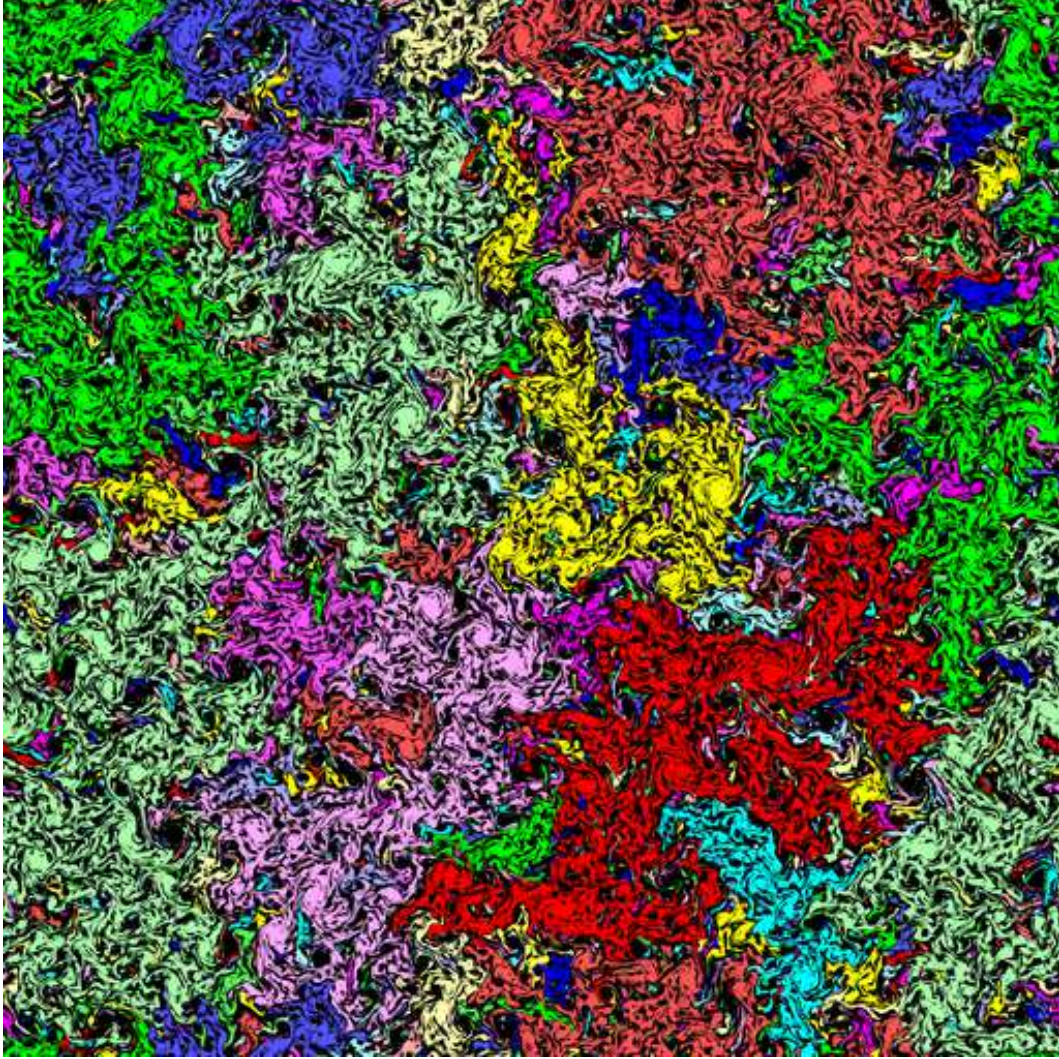


FIG. 1: Vorticity clusters. These are defined as connected regions with the same sign of vorticity (here positive). Colours are arbitrarily attributed to different clusters. Regions of negative vorticity are black. The forcing lengthscale L_f is one hundredth of the box side.

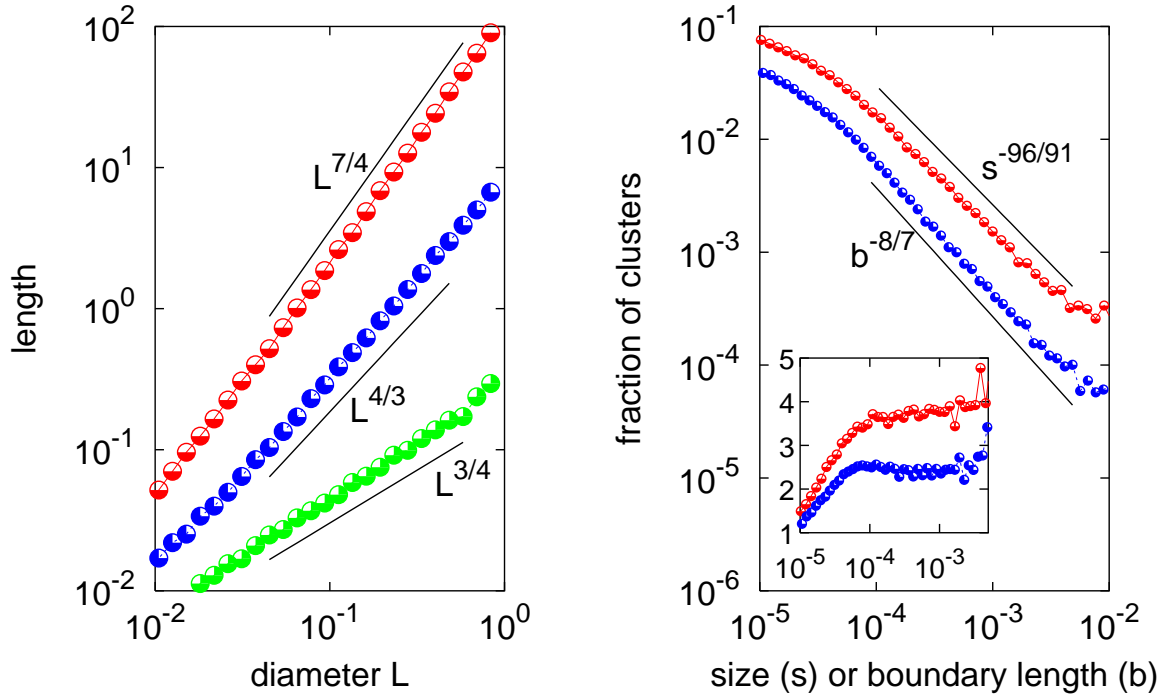


FIG. 2: Fractal dimensions and probabilities of size and boundary length for vorticity clusters. *Left panel:* The fractal dimensions are the slopes of the length-diameter dependencies in log-log coordinates for the boundary of filled clusters (red), for the outer boundary (blue) and for the necks of large fjords/peninsulae (green). The solid lines have slopes with the exact values for SLE_6 curves, $7/4$, $4/3$, $3/4$, respectively. Fractal dimensions are obtained by computing the average length for a given diameter of the cluster. *Right panel:* The fraction of clusters with sizes between s and $1.25s$ (red symbols) and with boundary lengths between b and $1.25b$. The solid lines are the predictions from the percolation theory. Inset shows the same data multiplied by $s^{96/91}$ and $b^{8/7}$, respectively. The vertical scale is linear to appreciate the plateau in the compensated plot.

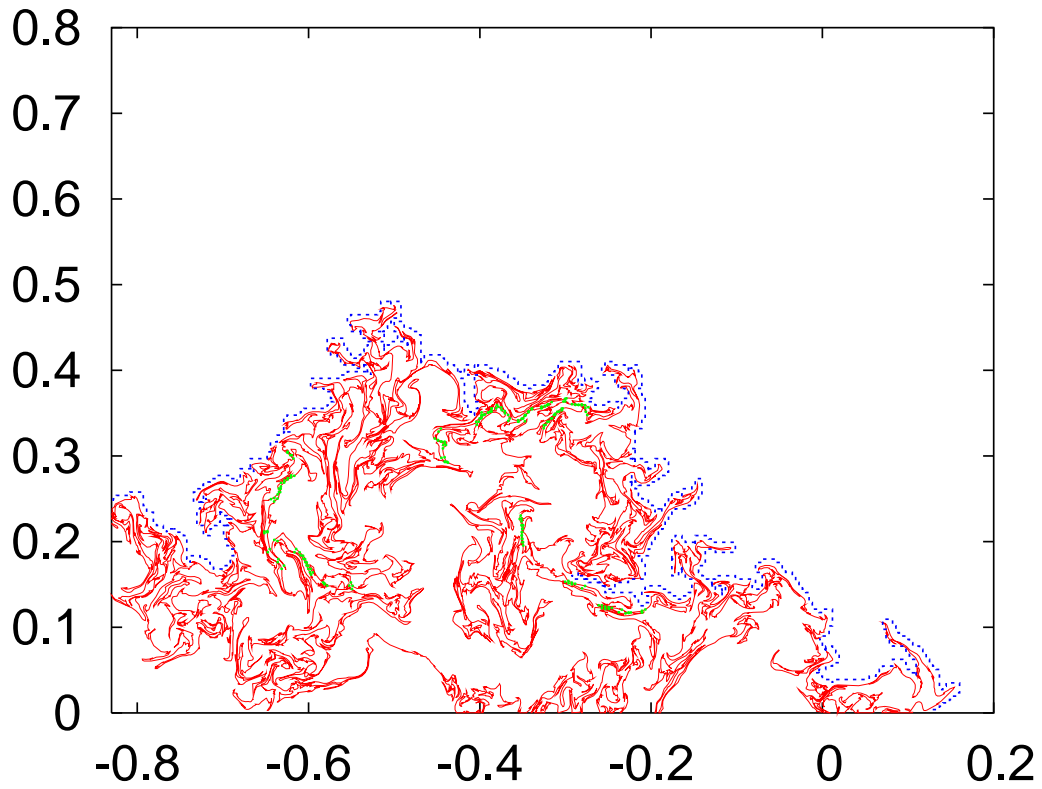


FIG. 3: A portion of a candidate SLE trace obtained from the vorticity field. The red curve is a zero-vorticity line in the upper half-plane. The dashed blue line is the "outer boundary" of the red curve, i.e. the boundary of the region that can be reached from infinity without getting closer than L_f to the red curve. The green dots mark the necks of large fjords and peninsulae.

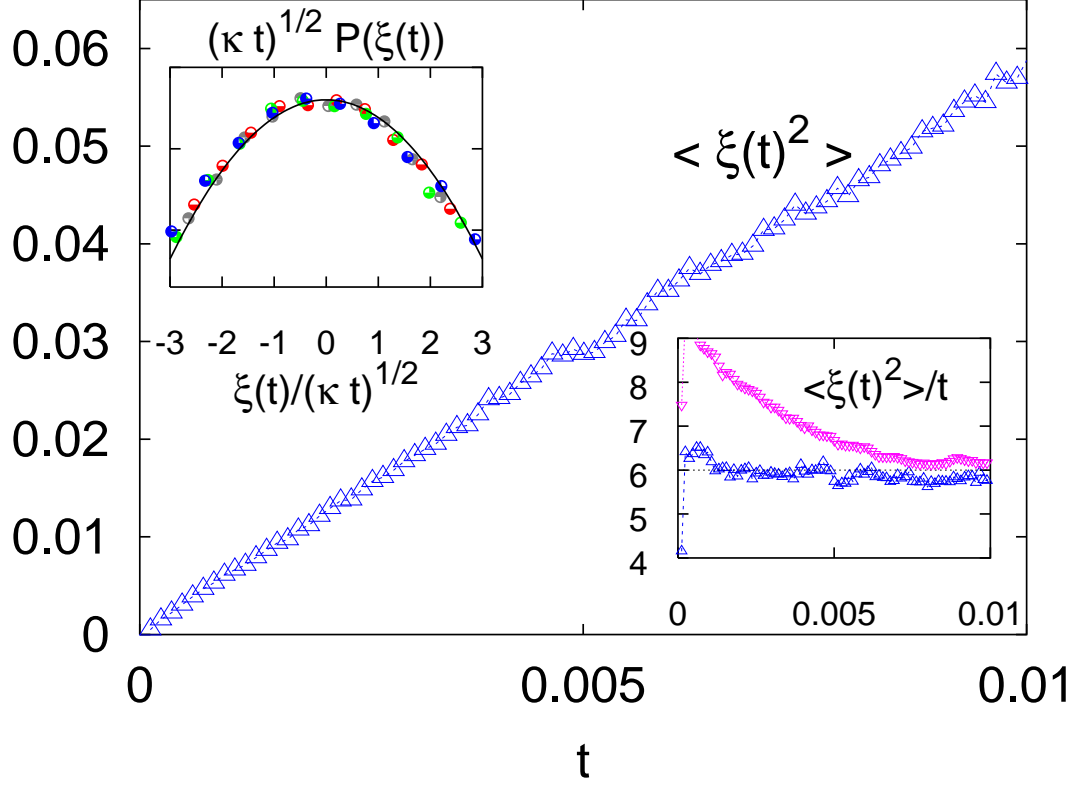


FIG. 4: The driving function is an effective diffusion process with diffusion coefficient $\kappa = 6 \pm 0.3$. The inverse cascade range corresponds to $5 \cdot 10^{-5} < t < 10^{-2}$. *Main frame*: the linear behaviour of $\langle \xi(t)^2 \rangle$. *Lower-right inset*: Diffusivity: blue for vorticity isolines, pink for the field with randomized phases. *Upper-left inset*: the probability density function of the rescaled driving function $\xi(t)/\sqrt{\kappa t}$ at four different times $t = 0.0012, 0.003, 0.006, 0.009$; the solid line is the Gaussian distribution $g(x) = (2\pi)^{-1/2} \exp(-x^2/2)$.

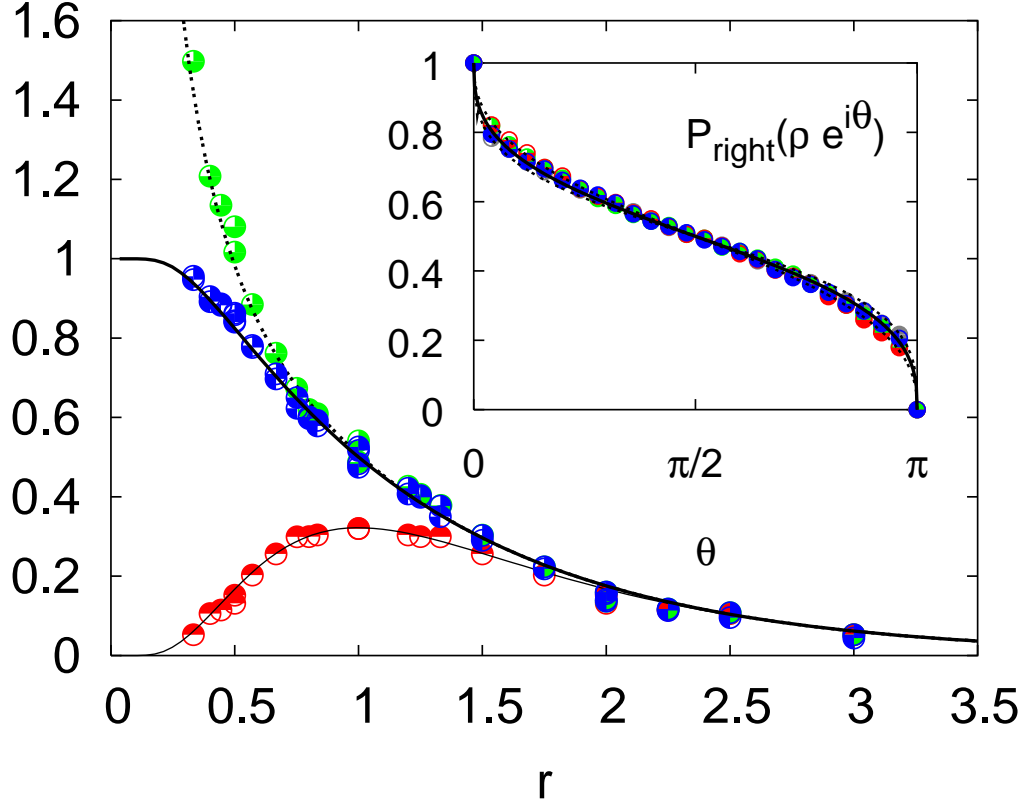


FIG. 5: Crossing and surrounding probability for vorticity clusters. *Main frame*: the probability π_v that a cluster crosses from top to bottom a rectangle of aspect ratio r (blue), the average number N_v of vertically crossing clusters (green), and the probability π_{hv} of a "four-legged" cluster joining all sides of the rectangle (red). The lines are the exact results for $\kappa = 6$: $\pi_v = \frac{3\Gamma(\frac{2}{3})}{\Gamma(\frac{1}{3})^2} \eta^{1/3} {}_2F_1\left(\frac{1}{3}, \frac{2}{3}; \frac{4}{3}; \eta\right)$ with $\eta = [(1-k)/(1+k)]^2$ and $r = K(1-k^2)/[2K(k^2)]$ (Cardy-Smirnov, thick solid line); $N_v = \frac{1}{2}[\pi_v + \pi_{hv} - \frac{\sqrt{3}}{2\pi} \log \eta]$ (Cardy, thick dashed line); $\pi_{hv} = \pi_v - \frac{\eta}{\Gamma(\frac{2}{3})\Gamma(\frac{1}{3})} {}_3F_2\left(1, 1, \frac{4}{3}; 2, \frac{5}{3}; \eta\right)$ (Watts-Dubédat, thin dotted line). *Inset*: the probability that a zero-vorticity line in the upper half-plane leaves the point $\rho e^{i\theta}$ to its right, for $\rho = 0.048, 0.064, 0.080, 0.096$. The prediction for SLE $_{\kappa}$ traces is $P = \frac{1}{2} + \frac{\Gamma(\frac{4}{\kappa})}{\sqrt{\pi}\Gamma(\frac{8-\kappa}{2\kappa})} {}_2F_1\left(\frac{1}{2}, \frac{4}{\kappa}; \frac{3}{2}; -\cot^2 \theta\right) \cot \theta$, shown as a thick solid line for $\kappa = 5.9$ (the best fit). The dashed lines are the probabilities for $\kappa = 5.7$ and $\kappa = 6.1$.

N	dx	ν	α	u_{rms}	L_f	ℓ_d	ε_I	ε_ν	ε_α	η_I	η_ν	η_α
2048	4.9×10^{-4}	2×10^{-5}	0.015	0.26	0.01	2.4×10^{-3}	3.9×10^{-3}	1.8×10^{-3}	2.1×10^{-3}	39.3	38.0	1.3
4096	2.4×10^{-4}	5×10^{-6}	0.024	0.26	0.01	1.2×10^{-3}	3.9×10^{-3}	0.7×10^{-3}	3.2×10^{-3}	39.3	36.1	3.2
8192	1.2×10^{-4}	2×10^{-6}	0.025	0.27	0.01	7.8×10^{-4}	3.9×10^{-3}	0.3×10^{-3}	3.6×10^{-3}	39.3	35.3	4.0
16384	0.6×10^{-4}	1×10^{-6}	0.0	0.24	0.01	5.5×10^{-4}	3.8×10^{-3}	0.2×10^{-3}	3.6×10^{-3}	39.5	37.6	1.9

TABLE I: Parameters of the simulations. N spatial resolution, dx grid spacing, ν viscosity, α friction, L_f forcing scale, $\ell_d = \nu^{1/2}/\eta_\nu^{1/6}$ enstrophy dissipative scale, ε_I energy injection rate, ε_ν viscous energy dissipation rate, ε_α energy dissipation by large-scale friction (energy growth rate for $N = 16384$), η_I enstrophy injection rate, η_ν viscous enstrophy dissipation rate, η_α enstrophy dissipation by friction (enstrophy growth rate for $N = 16384$).